NANO LETTERS

Letter

pubs.acs.org/NanoLett

High-Efficiency Nanostructured Window GaAs Solar Cells

Dong Liang,[†] Yangsen Kang,[‡] Yijie Huo,[‡] Yusi Chen,[‡] Yi Cui,[§,⊥,*] and James S. Harris*[,‡,§,∥]

[†]Department of Physics, [‡]Department of Electrical Engineering, [§]Department of Materials Science and Engineering, and [∥]Department of Applied Physics Stanford University, Stanford, California 94305, United States

[⊥]SLAC National Accelerator Laboratory, Stanford Institute for Materials and Energy Sciences, Menlo Park, California 94205, United States

ABSTRACT: Nanostructures have been widely used in solar cells due to their extraordinary optical properties. In most nanostructured cells, high short circuit current has been obtained due to enhanced light absorption. However, most of them suffer from lowered open circuit voltage and fill factor. One of the main challenges is formation of good junction and electrical contact. In particular, nanostructures in GaAs only have shown unsatisfactory performances (below 5% in energy conversion efficiency) which cannot match their ideal material properties and the record photovoltaic performances in industry. Here we demonstrate a completely new design for nanostructured solar cells that combines nanostructured window layer, metal mesa bar contact with small area, high quality planar junction. In this way, we not only keep the advanced optical properties of nanostructures such as broadband and wide angle antireflection, but also minimize its negative impact on electrical properties. High light absorption, efficient carrier collection, leakage elimination, and good lateral conductance can be simultaneously obtained. A nanostructured window cell using GaAs junction and AlGaAs nanocone window demonstrates 17% energy conversion efficiency and 0.982 V high open circuit voltage.

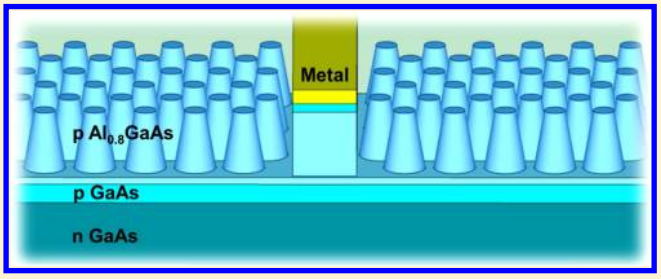

KEYWORDS: *GaAs, nanostructure, window layer, antireflection, solar cell*

Nanostructures have been widely applied to solar cells for antireflection coatings,[1] light trapping absorbers,[2−11] core−shell radial p−n junctions,[6−14] back reflectors,[15,16] quantum tuning,[17] improved charge transport,[18] and so forth. Most of these devices have demonstrated enhanced short circuit current density (J_{sc}) due to advanced antireflection and light trapping effects. However, nanostructures also increase the surface area and the number of defects, which results in lower open circuit voltage (V_{oc}) fill factor (FF) and efficiency. Despite quite major efforts to solve these problems,[2,3,12] they remain significant challenges to utilizing nanostructures to achieve higher efficiency. Here we demonstrate the application of a centimeter-scale array of nanocones on an AlGaAs window layer GaAs solar cell, resulting in a high V_{oc} (0.982 V) and a high J_{sc} (24.4 mA/cm^2), leading to a 17.0% energy conversion efficiency. Different from previous approaches to nanostructuring the absorbers,[2−18] nanostructuring the window layer not only increases optical absorption and photocurrent but also improves solar cell electrical performance parameters of voltage, fill factor, and efficiency due to preserved junction quality, enhanced carrier confinement, surface passivation, and reduced series resistance and shunt conductance.

A window layer is a layer of wide band gap, optically transparent material, which is generally lattice matched to the absorber to produce an interface with low recombination and carrier confinement. Window layers are widely used in a variety of optoelectronic devices, such as solar cells,[19−22] LEDs,[23] and detectors.[24] In solar cells specifically, the window layer is a quasi-transparent conducting layer with a large bandgap, sandwiched between the antireflection layer and the emitter. They are most often found in compound semiconductor solar cells, such as III−V,[19,20] CdTe,[21] and CIGS[22] solar cells. Typical window layer materials include CdS, ZnS, and ZnO for CdTe and CIGS solar cells, $Al_{0.8}Ga_{0.2}As$ and $In_{0.51}Ga_{0.49}P$ for GaAs solar cells, and so forth. Ideally, a window layer should be highly transparent across the entire solar spectrum. Practically, due to their finite bandgap, photons with energy above the bandgap are inevitably absorbed by the window layer itself. In order to minimize this self-absorption, the window layer thickness is typically less than 100 nm. However, if their bandgap is sufficiently large, it can be much thicker. For example, ZnO can be several micrometers thick on thin film a-Si solar cells.[15] In another scenario, if the absorbed light in the window layer can be converted into photo current, the layer can be relatively thick to provide greater lateral conductance and smaller shunt conductance. Thus, there is plenty of room to engineer the window layer design to extend its functionalities.

Here we demonstrate a "nanowindow" solar cell that combines a nanostructured window layer with a planar absorber/junction. In addition to carrier confinement and higher lateral conductance, this nanostructured window layer

Received: July 20, 2013
Revised: September 6, 2013
Published: September 10, 2013

   dx.doi.org/10.1021/nl402680g | *Nano Lett.* 2013, 13, 4850−4856

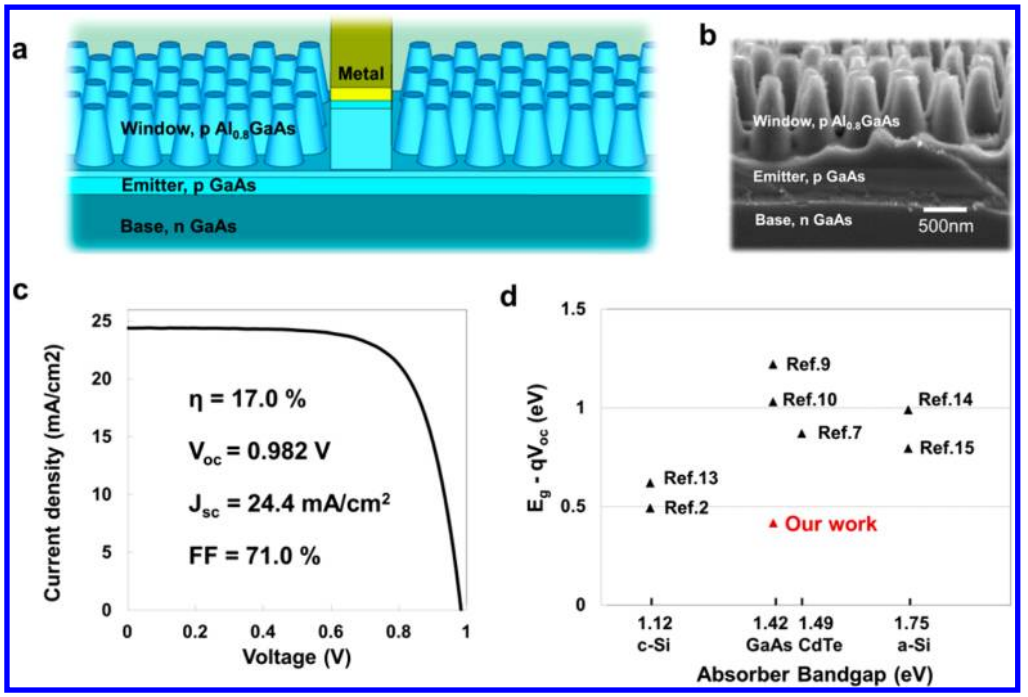

Figure 1. Overview of an AlGaAs/GaAs nanostructured window solar cell. (a) Schematic of the device structure. (b) SEM cross-section image of the solar cell active region with $Al_{0.8}Ga_{0.2}As$ nanocone window layer. (c) 1 Sun $J-V$ characterizations of the best sample (sample area is 0.50 cm^2). (d) band gap-voltage offset ($E_g/q - V_{oc}$) for several published nanostructured solar cells with absorber materials of c-Si, GaAs, CdTe, and a-Si.

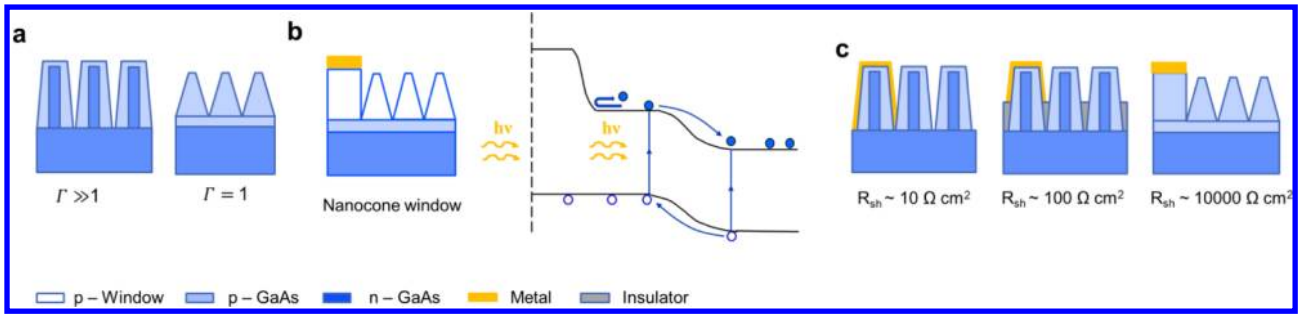

Figure 2. Novel design elements incorporated into the nanostructured window solar cell compared to a radial junction nanopillar/nanowire solar cell. (a) Junction. Left: high aspect ratio radial p–n junction has a high junction/footprint ratio $\Gamma \gg 1$. Right: planar junction has $\Gamma = 1$. (b) Left: Nanostructured window layer with separate nonstructured ohmic contact region. Right: band diagram of a nanocone window solar cell. (c) Contact designs. Left: direct deposition of metal on nanostructured surface in radial junction nanopillar solar cell. Middle: adding insulating layer deposited into nanostructure valleys in radial junction nanopillar solar cell. Right: separate metal contact from nanostructured region in nanostructured window solar cell.

serves as a broadband, angle-independent antireflection layer, thus eliminating the need for multilayer antireflection coatings, such as the MgF_2/ZnS bilayer coating commonly used for GaAs solar cells. We demonstrate that both the optical and electrical properties in a nanostructured solar cell are enhanced simultaneously.

Figure 1a is a schematic illustration of our $Al_{0.8}Ga_{0.2}As$ nanocone window layer GaAs solar cell. The $Al_{0.8}Ga_{0.2}As$ nanocone arrays are created on top of a planar GaAs p–n junction. The AlGaAs nanocones serve as an antireflection layer and window layer simultaneously. Figure 1b shows a 10° tilted cross-section scanning electron microscope (SEM) image of the AlGaAs nanocones that are etched between mesa bar ohmic contacts. Each nanocone is ~900 nm high and ~650 nm in diameter. Figure 1c shows the photocurrent density versus voltage ($J-V$) curves measured under AM 1.5G normal illumination (1000 W/m^2, 1 sun) at room temperature, where J_{sc} = 24.4 mA/cm^2, V_{oc} = 0.982 V, FF = 71% and the overall energy conversion efficiency, η = 17.0%. This is compared to efficiencies of less than 5% for previously reported nanostructured GaAs solar cells[9,10] due to degraded V_{oc} and FF. This AlGaAs/GaAs nanostructured window solar cell demonstrates both enhanced optical and electrical properties, thus not only high photocurrent was achieved, but also high V_{oc}, FF, and overall efficiency. Figure 1d is a plot of the band gap-voltage offset ($E_g - qV_{oc}$) for a number of published nanostructured solar cells with absorbers of c-Si, GaAs, CdTe, and a-Si against their bandgap E_g. Our nanostructured window solar cell has a V_{oc} only 0.438 V lower than the GaAs bandgap (1.42 eV). In another AlGaAs/GaAs nanostructured window cell, we achieved a V_{oc} of 1.003 V, only 0.417 V lower than the GaAs bandgap, though the overall efficiency was 16.3%, slightly lower than the cell reported in Figure 1. The small band gap-voltage offset reflects a low nonradiative recombination loss in our AlGaAs/GaAs nanostructured window solar cells. We believe that by optimizing our doping levels and growth conditions, V_{oc}

dx.doi.org/10.1021/nl402680g | Nano Lett. 2013, 13, 4850–4856

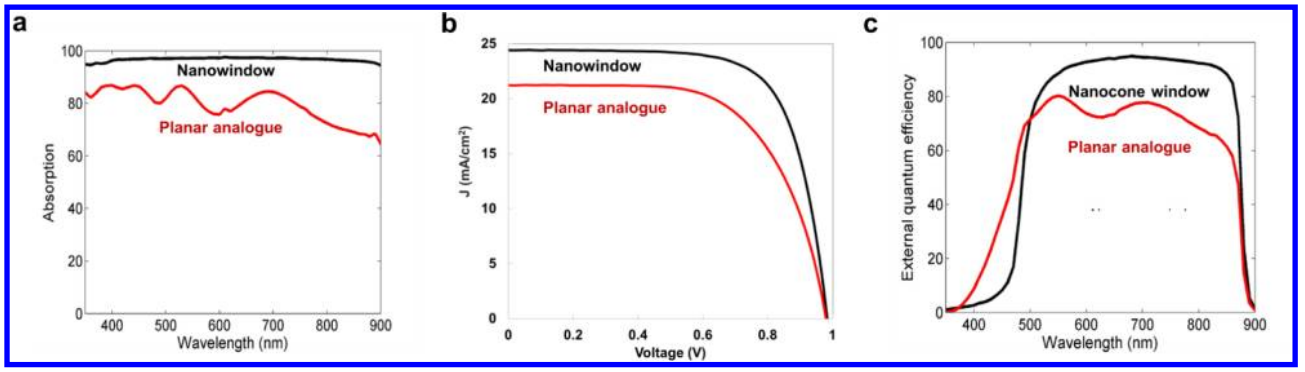

Figure 3. Comparison of measured properties of the AlGaAs/GaAs nanostructured window solar cell (black) and planar analogue sample (red). (a) Optical absorption. (b) $J-V$ characteristic. (c) External quantum efficiency (EQE).

and efficiency for a nanostructured window solar cell can compete with the very best planar solar cells.[25]

Comparison with Conventional Nanostructured Solar Cells. The high V_{oc} and FF benefit from both the smaller junction area and a lower dark current density by avoiding defects in nanostructured junctions compared to typical nanostructured solar cells. Figure 2a shows a structural comparison of our nanocone window solar cell with a conventional nanostructured radial p−n junction cell. Without considering parasitic resistances, V_{oc} is given by[26]

$$V_{oc} = \frac{mk_BT}{q} \ln\left[\left(\frac{J_{sc}}{J_0\Gamma}\right) + 1\right] \quad (1)$$

where m is the junction ideality factor, J_0 is the saturation current density, and J_{sc} is the photocurrent density with respect to the planar area, which is a constant assuming 100% external quantum efficiency above the absorber bandgap at 1 sun illumination. Γ is the ratio of total junction area to planar area, that is, the cylindrical junction to the planar base area. The higher the value of Γ, the greater the decrease in V_{oc}. As shown in Figure 2a, a conventional nanostructured radial p−n junction solar cell has $\Gamma \gg 1$ while a nanostructured window layer cell with a planar junction has $\Gamma = 1$. For a nanowire core−shell p−n junction solar cell with a core diameter of 50 nm and a height of 5000 nm, $\Gamma = 100$, corresponding to 0.119 V loss in V_{oc}, which is significant compared to the 600 to 1000 mV V_{oc} for typical cells, resulting in a 10−20% efficiency loss. Relocating nanostructures from the depletion region of p−n junction to the window layer avoids such degradation. In addition to this work, the effect of nanostructuring in solar cells with similarly small values of Γ has been observed in other recently reported high efficiency and high V_{oc} nanostructured solar cells, such as the black silicon cell with a quasi-planar junction[2] ($\Gamma > \sim 1$) and axial junction InP nanowire solar cells[3] ($\Gamma = 0.12$) . All of these nanostructured solar cells have two common elements similar to our design in addition to nanostructuring: junctions of much lower area and either separated from or minimally intersecting the nanostructured region.

In addition to the small junction area, higher quality junctions from material with long lifetime and diffusion length lead to lower saturation current, J_0, which also leads to higher V_{oc}. For conventional radial p−n junction nanostructured solar cells, the lifetime and diffusion length can be seriously degraded by increased defects if the junction is grown on a nanostructured template. It can also be limited by the radial layer thickness of the wire structure. This drawback is more significant in single crystalline materials with long diffusion lengths, such as GaAs, compared to polycrystalline or amorphous materials. By moving the nanostructured region from the p−n junction to the window layer, the lifetime, and diffusion length degradation due to nanostructuring is avoided.

The high J_{sc} is attributed to the nanocone antireflection properties and window layer carrier confinement. While nanocones can suppress reflection, surface recombination in the nanocone absorber may kill most of the minority carriers in the nanocones before they are collected, causing a lowered J_{sc}. To avoid this penalty, Figure 2b shows that instead of using the same absorber material in the nanocones, using a wider bandgap window material allows most of light to transmit through the window layer. The nanostructured window produces a wave guiding effect so that the carriers are created sufficiently close to junction to be very effectively collected. In addition, the window layer provides a barrier that confines the minority carriers from going to the surface. Figure 2b shows the band diagram of a nanostructured window solar cell. If an electron in the p-type emitter is diffusing toward the surface instead of the junction, the window barrier will reflect the electron back toward the junction so that it can be collected. Even for carriers generated by short wavelength light in the nanostructured window layer due to lower surface recombination velocity of the window material, they have a greater chance to be collected and contribute to the absorber photocurrent. A good fill factor is mainly attributed to a low series resistance and a high shunt resistance. In terms of series resistance, our contact design ensures a continuous metal film across the metal grids as opposed to a metal film with discontinuities that can occur on a nanostructured surface. Also the nanostructured window layer provides additional lateral conductance. The shunt resistance extracted from the $J-V$ curve of our nanostructured window cell is approximately 1×10^4 Ω cm^2. This result demonstrates the benefit of separating the metal contact from the nanostructured surface by simply not nanostructuring the ohmic contact region. The left picture in Figure 2c shows that direct deposition of metal on a nanostructured surface results in parasitic shunts. Together with a less uniform junction, a shunt resistance on the order of 10 Ω cm^2 is expected (based on our previous experiments) leading to typical FF of ∼0.25 and V_{oc} of only ∼0.5 V (GaAs cells). Adding an insulating layer, such as SiO_x[9] or benzocyclobutene (BCB)[10] into the valleys between the nanostructures reduces these shunts in the valleys, improving the shunt resistance to ∼10^2 Ω cm^2, FF up to ∼0.6, and V_{oc} to ∼0.95 V. In contrary, our mesa contact design (rightmost

dx.doi.org/10.1021/nl402680g | Nano Lett. 2013, 13, 4850−4856

structure in Figure 2c) for the nanostructured window solar cell completely separates the metal contact from the nanostructured region. This contact design and planar junction result in a shunt resistance of $\sim 10^4$ Ω cm^2, sufficiently high so that shunt resistance is no longer a limiting factor for FF and V_{oc}.

Comparison of Nanostructured Window and Planar Cells. For comparison, an identical planar junction cell was fabricated with the exception that a 100 nm thick flat window layer was used rather than the thicker nanostructured window layer. All other parameters were identical to the nanostructured cell. Figure 3a shows the optical absorption of a nanocone AlGaAs window solar cell compared to the planar control cell, measured with a standard integrating sphere. The nanostructured window cell achieves absorption of about 97% across the entire solar spectrum from 400 to 880 nm. Because AlGaAs has a similar refractive index to GaAs, there is almost no reflection loss at the window/absorber interface. The reflection loss from the window/air interface is minimized by the nanocones that provide a gradual change in the effective refractive index from n_{air} = 1 at their tip to n_{bulk} = 3.5 at the bottom. With our previously reported large acceptance angle nanostructures,[5] the improvement in total photon absorption throughout the day can be significantly larger in the nanostructured window solar cell when operating in a flat-plate, nontracking system.

Figure 3b shows the 1 sun $J-V$ characterizations of both the nanostructured window cell and the planar cell. Their parameters are summarized in Table 1. Compared to the planar control, J_{sc} in the nanostructured cell is improved by 15% from 21 to 24 mA/cm^2. V_{oc} is also slightly increased from 0.979 to 0.982 V, attributed to the larger photocurrent. The FF is improved from 63 to 71%, due to the thicker window layer that results in series resistance, decreasing from 5.8 to 3.9 Ω cm^2. The nanostructured AlGaAs window is thicker on average than its planar counterpart thus has better lateral conductance. The overall energy conversion efficiency is increased from 13.1 to 17.0%, which in total is a 30% improvement. When including the improved absorption due to the large nanocone acceptance angle, the improvement in electricity yield throughout the day can be greater than 30%.

Table 1. Parameter Improvements in a Nanocone Window Solar Cell Compared with a Planar Control Cell

	V_{oc}	J_{sc}	FF	efficiency
planar cell	0.979 V	21.23 mA/cm^2)	63.1	13.1%
nanocone window cell	0.982 V	24.40 mA/cm^2	71.0	17.0%
improvement	0.3%	15%	13%	30%

To further analyze the spectral response of the photocurrent, external quantum efficiency (EQE) was measured for both cells as shown in Figure 3c. Compared to the planar control cell, the EQE of the nanostructured window cell is significantly enhanced between 500 nm and 880 nm, reaching over 90%, indicating efficient charge separation at these wavelengths, that is, high internal quantum efficiency, benefiting from carrier confinement by the window barrier. Integrating the measured EQE with 1.5 AM solar spectrum for both cells results in approximately 15% difference in their total photocurrents, which matches the J_{sc} improvement in $J-V$ measurement. According to the number of absorbed photons calculated from the measured optical absorption, J_{sc} could be 31 mA/cm^2 assuming 100% internal quantum efficiency (the Shockley–Queisser limit is 32.4 mA/cm^2), higher than the measured 24.4 mA/cm^2. The loss is caused by recombination in AlGaAs window at wavelengths below 500 nm, making the nanostructured window EQE lower than the planar cell in the blue spectral region. This is an expected trade-off because the AlGaAs bandgap is still relatively small compared to an ideal window bandgap of 3–4 eV. However, assuming the carriers generated in the AlGaAs nanocones themselves completely recombine, the improvement in J_{sc} would be only ~22 mA/cm^2. This implies that a significant fraction of the short wavelength photons absorbed in the AlGaAs nanostructured window layer actually contribute to the photocurrent. To find more support for this argument, light absorption in AlGaAs nanocone window and in GaAs active layer are simulated with Finite Difference Time-Domain (FDTD)[27] simulator and plotted against experimental EQE shown in Figure 4a. The

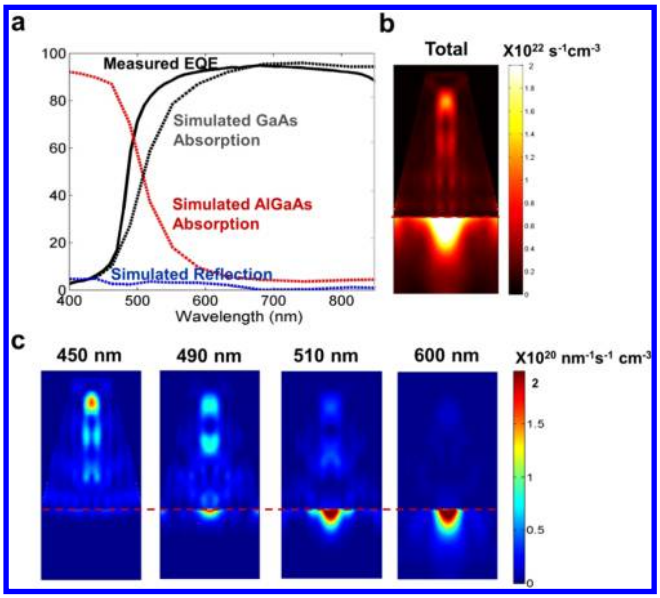

Figure 4. FDTD simulation of absorption in an AlGaAs nanocone window and bulk GaAs. (a) Evidence of photocurrent contribution from electron–hole pairs created in the AlGaAs nanocone window. Measured EQE of the nanostructured window cell (black solid line), simulated light absorption in the AlGaAs nanocone window (red dashed line), absorption in the GaAs absorber (black dashed line) and reflection (blue dashed line). (b) Simulated cross sectional mappings of total photon absorption rates integrated from 350 to 900 nm and (c) at 450, 490, 510, and 600 nm. The red dashed lines indicate AlGaAs/GaAs interfaces.

simulated reflection (blue) matches the experimental measurement from the integrating sphere in Figure 3a: both are ~3%. According to the simulation, for wavelengths above 550 nm most of the absorption is in the GaAs (dashed black line) and almost none in the AlGaAs nanocone window (dashed red line). Therefore, photocurrent at these wavelengths is from the light absorbed in the GaAs. However, at wavelengths near 500 nm, the EQE (solid black line) is much higher than the absorption in GaAs. This offset between EQE and absorption simulation suggests carriers transferring from the AlGaAs nanocones to the GaAs junction, which partially compensates for the expected loss in the AlGaAs. For example, the EQE at 477 nm is 30%, while absorption in the GaAs is less than 10%, thus more than two-thirds of the photocurrent is contributed by carriers generated in and collected from the AlGaAs

dx.doi.org/10.1021/nl402680g | Nano Lett. 2013, 13, 4850–4856

nanocones. The EQE at 490 nm is 59%, while the GaAs absorption is only 27%, thus over half of the photocurrent is from the AlGaAs nanostructured window. At 510 nm, more than one-third of the 78% EQE is from the AlGaAs.

Figures 4b,c shows cross sectional maps of the light absorption distribution, which also represents the distribution of generated electron−hole pairs. Figure 4b shows the absorbed photon density integrated from 350 to 900 nm while Figure 4c shows absorption mappings at different wavelengths. The AlGaAs nanocone window transfers most of the incident light into the region below it, where a cluster of highly concentrated photons is observed. The carriers excited by absorption near the bottom of the nanocones tend to diffuse down into the GaAs p−n junction while those in the top of the cone where electron−hole pairs are closer to the surface largely recombine. As wavelength increases, absorption tends to shift downward, as shown in Figure 4c.

The major loss mechanism is recombination in the nanostructured window layer, which limits the total photocurrent. This loss causes the efficiency gap between our nanostructured window solar cell and best GaAs planar solar cell. However, with higher bandgap window materials this gap could be closed. Considering potentially better angle performance, the nanostructured window solar cell could eventually outperform the current best planar solar cell, especially in electricity throughput without tracking systems. Other loss mechanisms include light reflection and carrier recombination at window/bulk interface. To search for better material candidates for a nanostructured window layer, the following criteria need to be considered. First, the window refractive index needs to be very close to that of the absorber so that there is minimal light reflection at the interface of the window layer and the absorber. Overall perfect antireflection can be expected with an ideal tapered shape in the window nanostructure. Second, in single crystalline solar cells, it is favored that the lattice constant of the window layer matches the rest of the solar cell to ensure high interface quality and a low interface recombination rate in order to take the advantage of minority carrier confinement by the window barrier. Third, a wide band gap is preferable in general. If materials have the same bandgap, an indirect bandgap material is preferable versus a direct bandgap material. In our experiments, we have tried both $Al_{0.8}Ga_{0.2}As$ and $In_{0.51}Ga_{0.49}P$ for window materials. Their refractive indices and lattice constants all match GaAs. Both have wide band gaps and low surface recombination rates.[28] However, for the nanostructured window layer $Al_{0.8}Ga_{0.2}As$ performs much better because it is an indirect band gap material while $In_{0.51}Ga_{0.49}P$ is direct bandgap. Although $Al_{0.8}Ga_{0.2}As$ has a band gap of 2.09 eV, corresponding to 593 nm in wavelength, its absorption edge is actually at 480 nm, which corresponds to its direct band gap of 2.59 eV at the Γ valley.[29] In contrast, $In_{0.51}Ga_{0.49}P$ has a sharp absorption edge at 650 nm, corresponding to its actual bandgap of 1.90 eV. Our measurements show much higher short wavelength EQE in an $Al_{0.8}Ga_{0.2}As$ nanostructured window solar cell compared to an $In_{0.51}Ga_{0.49}P$ nanostructured window cell.

Other materials to explore include AlInP whose bandgap is up to 2.4 eV and some II−VI compounds lattice-matched to a (100) GaAs substrate with 3−4 eV bandgap. Moreover, a graded AlGaAs nanostructured window with a gradual change of Al concentration from the top surface of nanostructure to the emitter could enhance the short wavelength performance by providing an electric field in the nanostructured window to enhance carrier collection. Nanostructuring window layer is certainly not limited to III−V solar cells but is also applicable to other material systems such as CdTe/CdS solar cells with a CdTe planar absorber and CdS nanostructured window.

In summary, we have demonstrated a nanostructured window solar cell using an AlGaAs nanocone window layer on a GaAs planar junction, which achieved 17% efficiency. This is the highest reported efficiency among all III−V nanostructured solar cells. Importantly, the nanostructured window design provides high quality planar junctions that avoid the fundamental V_{oc} and FF degradation in traditional nanostructured junction solar cells. A record V_{oc} of 1.003 V was achieved in one of our AlGaAs/GaAs nanostructured window cells. This value of V_{oc} is also very close to the absorber's bandgap (offset 0.42 V). Optically, the nanostructured window material has a refractive index that is nearly equal to that of the bulk material, thus there is no reflection at the window/bulk interface. Tapered nanostructures with gradual change of refractive indices from air to bulk produce an excellent, antireflection interface. Electrically, the nanostructured window is lattice matched to the bulk but with a wider bandgap, therefore, it confines the minority carriers within the junction and significantly reduces surface recombination. Enhanced light absorption and carrier confinement lead to high J_{sc}. In addition, the mesa contact design avoids potential shunts from a nanostructured surface and results in a high FF. Finally, the indirect bandgap nature of AlGaAs makes it a good choice for the nanostructured window material for GaAs solar cells. Other materials are possible to even close the efficiency gap between nanostructured window solar cells and the best planar counterparts.

Methods. *Solar Cell Fabrication.* A GaAs solar cell with an AlGaAs window was first grown on an n-type GaAs substrate by metal organic chemical vapor deposition (MOCVD). The solar cell structure includes the following: a 100 nm p-type heavily doped GaAs 2.5×10^{19} cm^{-3} as a contact layer, a 1100 nm thick p-type $Al_{0.8}Ga_{0.2}As$ window layer with doping of 2×10^{18} cm^{-3}, whose extra thickness was designed for the subsequent nanocone etching, a 300 nm thick GaAs emitter with p-type doping of 1×10^{18} cm^{-3}, a 3000 nm GaAs base with n-type doping of 2×10^{17} cm^{-3} plus a 50 nm thick back side field (BSF) layer of n-type $Al_{0.3}Ga_{0.7}As$. All the III−V layers were deposited at 720 C. After MOCVD growth, a multilayer alloy film of Au/Ge/Ni/Au (40 nm/12 nm/12 nm/80 nm) was e-beam evaporated as the back electrode. Metal fingers of Ti/Pt/Au (40 nm/40 nm/80 nm) alloy were deposited as the top electrodes.

Nanostructured AlGaAs Window Fabrication. Periodic AlGaAs nanocones were fabricated by nanosphere masking. First, Langmuir−Blodgett assembly of monodispersed SiO_2 nanospheres were coated on top of the GaAs solar cell with patterned metal grids. During the coating, the orientation of the metal fingers were aligned vertically to avoid disruption of the surface tension during wafer emersion. The monolayer of nanospheres together with the metal fingers were then used as a mask for chlorine-based electron cyclotron resonance-reactive ion etching (ECR-RIE) of the AlGaAs layer, forming mesa grids with AlGaAs nanocones in between. The metal grids and nanospheres both serve as the mask of nanostructure etching, which is the key difference from our previously described methods.[5] The etching was stopped when there was about 50 nm of the AlGaAs layer left under the nanocones to maintain their lateral continuity and full coverage of the GaAs surface.

dx.doi.org/10.1021/nl402680g | Nano Lett. 2013, 13, 4850−4856

After that, the device was dipped into an ammonium and hydroperoxide solution to reduce surface roughness of the nanocone surfaces. The p+ GaAs contact layer is completed etched in the nanocones and only remains beneath the metal grids.

Device Characterizations. Absorption measurements were taken using a standard integrating sphere system. Incident light enters the sphere through a small port and illuminates the sample mounted in the center of the sphere. The reflected and transmitted light was scattered uniformly by the interior sphere wall. A silicon detector mounted at the back of the sphere produces a photocurrent of all the reflected and transmitted photons. With a reference photocurrent for the initial incident light, absorption can be calculated. $J-V$ was measured under AM 1.5 G normal illuminations (1000 W/m^2, 1 sun) at room temperature. A standard solar simulator was used as the light source whose intensity was monitored by a certificated solar cell. Series and shunt resistances were extracted from the *IV* slopes at the open circuit and the short circuit, respectively. EQE was measured shinning laser beam on the nanocone surface between mesa bar contacts. Devices were illuminated by mechanically chopped monochromatic light and the photocurrent was measured using a lock-in amplifier. The light intensity was calibrated with an amplified and calibrated Si photodetector. Solar cell J_{sc} was calculated based on the unmetalized area and was confirmed by the integration of the EQE spectrum.

AUTHOR INFORMATION

Corresponding Authors

*E-mail: yicui@stanford.edu.

*E-mail: harris@snow.stanford.edu.

Notes

The authors declare no competing financial interest.

ACKNOWLEDGMENTS

The authors acknowledge the financial support of the DoE Bay Area Photovoltaic Consortium (BAPVC), technical assistance of P.-S. Wong and M. Riaziat of OEpic for MOCVD growth, and use of the processing facilities in the Stanford Nanofabrication Facility supported by the NSF NNIN program.

REFERENCES

(1) Yu, P. C.; Chang, C. H.; Chiu, C. H.; Yang, C. S.; Yu, J. C.; Kuo, H. C.; Hsu, S. H.; Chang, Y. C. Efficiency Enhancement of GaAs Photovoltaics Employing Antireflective Indium Tin Oxide Nanocolumns. *Adv. Mater.* **2009**, *21*, 1618−+.

(2) Oh, J.; Yuan, H. C.; Branz, H. M. An 18.2%-efficient black-silicon solar cell achieved through control of carrier recombination in nanostructures. *Nat. Nanotechnol.* **2012**, *7*, 743−748.

(3) Wallentin, J.; Anttu, N.; Asoli, D.; Huffman, M.; Aberg, I.; Magnusson, M. H.; Siefer, G.; Fuss-Kailuweit, P.; Dimroth, F.; Witzigmann, B.; Xu, H. Q.; Samuelson, L.; Deppert, K.; Borgstrom, M. T. InP Nanowire Array Solar Cells Achieving 13.8% Efficiency by Exceeding the Ray Optics Limit. *Science* **2013**, *339*, 1057−1060.

(4) Kelzenberg, M. D.; Boettcher, S. W.; Petykiewicz, J. A.; Turner-Evans, D. B.; Putnam, M. C.; Warren, E. L.; Spurgeon, J. M.; Briggs, R. M.; Lewis, N. S.; Atwater, H. A. Enhanced absorption and carrier collection in Si wire arrays for photovoltaic applications. *Nat. Mater.* **2010**, *9*, 239−244.

(5) Liang, D.; Huo, Y. J.; Kang, Y.; Wang, K. X.; Gu, A. J.; Tan, M. Y.; Yu, Z. F.; Li, S.; Jia, J. Y.; Bao, X. Y.; Wang, S.; Yao, Y.; Wong, H. S. P.; Fan, S. H.; Cui, Y.; Harris, J. S. Optical Absorption Enhancement in Freestanding GaAs Thin Film Nanopyramid Arrays. *Adv. Energy Mater.* **2012**, *2*, 1254−1260.

(6) Garnett, E.; Yang, P. D. Light Trapping in Silicon Nanowire Solar Cells. *Nano Lett.* **2010**, *10*, 1082−1087.

(7) Fan, Z. Y.; Razavi, H.; Do, J. W.; Moriwaki, A.; Ergen, O.; Chueh, Y. L.; Leu, P. W.; Ho, J. C.; Takahashi, T.; Reichertz, L. A.; Neale, S.; Yu, K.; Wu, M.; Ager, J. W.; Javey, A. Three-dimensional nanopillar-array photovoltaics on low-cost and flexible substrates. *Nat. Mater.* **2009**, *8*, 648−653.

(8) Putnam, M. C.; Boettcher, S. W.; Kelzenberg, M. D.; Turner-Evans, D. B.; Spurgeon, J. M.; Warren, E. L.; Briggs, R. M.; Lewis, N. S.; Atwater, H. A. Si microwire-array solar cells. *Energy Environ. Sci.* **2010**, *3*, 1037−1041.

(9) Czaban, J. A.; Thompson, D. A.; LaPierre, R. R. GaAs Core-Shell Nanowires for Photovoltaic Applications. *Nano Lett.* **2009**, *9*, 148−154.

(10) Mariani, G.; Wong, P. S.; Katzenmeyer, A. M.; Leonard, F.; Shapiro, J.; Huffaker, D. L. Patterned Radial GaAs Nanopillar Solar Cells. *Nano Lett.* **2011**, *11*, 2490−2494.

(11) Zhu, J.; Hsu, C. M.; Yu, Z. F.; Fan, S. H.; Cui, Y. Nanodome Solar Cells with Efficient Light Management and Self-Cleaning. *Nano Lett.* **2010**, *10*, 1979−1984.

(12) Tang, J. Y.; Huo, Z. Y.; Brittman, S.; Gao, H. W.; Yang, P. D. Solution-processed core-shell nanowires for efficient photovoltaic cells. *Nat. Nanotechnol.* **2011**, *6*, 568−572.

(13) Tian, B. Z.; Zheng, X. L.; Kempa, T. J.; Fang, Y.; Yu, N. F.; Yu, G. H.; Huang, J. L.; Lieber, C. M. Coaxial silicon nanowires as solar cells and nanoelectronic power sources. *Nature* **2007**, *449*, 885−889.

(14) Kempa, T. J.; Cahoon, J. F.; Kim, S. K.; Day, R. W.; Bell, D. C.; Park, H. G.; Lieber, C. M. Coaxial multishell nanowires with high-quality electronic interfaces and tunable optical cavities for ultrathin photovoltaics. *Proc. Natl. Acad. Sci. U.S.A.* **2012**, *109*, 1407−1412.

(15) Hsu, C. M.; Battaglia, C.; Pahud, C.; Ruan, Z. C.; Haug, F. J.; Fan, S. H.; Ballif, C.; Cui, Y. High-Efficiency Amorphous Silicon Solar Cell on a Periodic Nanocone Back Reflector. *Adv. Energy Mater.* **2012**, *2*, 628−633.

(16) Ferry, V. E.; Verschuuren, M. A.; Li, H. B. B. T.; Schropp, R. E. I.; Atwater, H. A.; Polman, A., Improved red-response in thin film a-Si:H solar cells with soft-imprinted plasmonic back reflectors. *Appl. Phys. Lett.* **2009**, *95*.

(17) Sargent, E. H. Colloidal quantum dot solar cells. *Nat. Photonics* **2012**, *6*, 133−135.

(18) Huynh, W. U.; Dittmer, J. J.; Alivisatos, A. P. Hybrid nanorod-polymer solar cells. *Science* **2002**, *295*, 2425−2427.

(19) delValle, C. A.; Alcaraz, M. F. Performance of antireflecting coating-AlGaAs window layer coupling for terrestrial concentrator GaAs solar cells. *IEEE Trans. Electron. Dev* **1997**, *44*, 1499−1506.

(20) Li, N.; Lee, K.; Renshaw, C. K.; Xiao, X.; Forrest, S. R., Improved power conversion efficiency of InP solar cells using organic window layers. *Appl. Phys. Lett.* **2011**, *98*.

(21) Liu, P. A.; Singh, V. P.; Jarro, C. A.; Rajaputra, S., Cadmium sulfide nanowires for the window semiconductor layer in thin film CdS-CdTe solar cells. *Nanotechnology* **2011**, *22*.

(22) Hagiwara, Y.; Nakada, T.; Kunioka, A. Improved J(sc) in CIGS thin film solar cells using a transparent conducting ZnO: B window layer. *Sol. Energy Mater. Sol. Cells* **2001**, *67*, 267−271.

(23) Huang, K. H.; Yu, J. G.; Kuo, C. P.; Fletcher, R. M.; Osentowski, T. D.; Stinson, L. J.; Craford, M. G.; Liao, A. S. H. Twofold Efficiency Improvement in High-Performance Algainp Light-Emitting-Diodes in the 555−620 Nm Spectral Region Using a Thick Gap Window Layer. *Appl. Phys. Lett.* **1992**, *61*, 1045−1047.

(24) Chowdhury, U.; Wong, M. M.; Collins, C. J.; Yang, B.; Denyszyn, J. C.; Campbell, J. C.; Dupuis, R. D. High-performance solar-blind photodetector using an Al0.6Ga0.4N n-type window layer. *J. Cryst. Growth* **2003**, *248*, 552−555.

(25) Miller, O. D.; Yablonovitch, E.; Kurtz, S. R. Strong Internal and External Luminescence as Solar Cells Approach the Shockley-Queisser Limit. *IEEE J. Photovolt* **2012**, *2*, 303−311.

(26) Kayes, B. M.; Atwater, H. A.; Lewis, N. S., Comparison of the device physics principles of planar and radial p−n junction nanorod solar cells. *J. Appl. Phys.* **2005**, *97*.
(27) Taflove, A.; Hagness, S. C. *Computational Electrodynamics: The Finite Difference Time-Domain Method*; Artech House: Norwood, MA, 2000.
(28) Pearton, S. J.; Ren, F.; Hobson, W. S.; Abernathy, C. R.; Chakrabarti, U. K. Comparison of Surface Recombination Velocities in Ingap and Algaas Mesa Diodes. *J. Vac. Sci. Technol., B* **1994**, *12*, 142−146.
(29) Vurgaftman, I.; Meyer, J. R.; Ram-Mohan, L. R. Band parameters for III-V compound semiconductors and their alloys. *J. Appl. Phys.* **2001**, *89*, 5815−5875.